2

Soil Minerals

2.1 Ionic Solids

The chemical elements making up soil minerals occur typically as ionic species with an electron configuration that is unique and stable regardless of whatever other ions may occur in a mineral structure. The attractive interaction between one ion and another of opposite charge nonetheless is strong enough to form a chemical bond, termed an *ionic bond*. Ionic bonds differ from covalent bonds, which involve a significant distortion of the electron configurations (*orbitals*) of the bonding atoms that results in the sharing of electrons. Electron sharing mixes the electronic orbitals of the atoms, so it is not possible to assign to each atom a unique configuration that is the same regardless of the partner with which the covalent bond has formed. This loss of electronic identity leads to a more coherent fusion of the orbitals that makes covalent bonds stronger than ionic bonds.

Ionic and covalent bonds are conceptual idealizations that real chemical bonds only approximate. In general, a chemical bond shows some degree of ionic character and some degree of electron sharing. The Si–O bond, for example, is said to be an even partition between ionic and covalent character, and the Al–O bond is thought to be about 40% covalent, 60% ionic. Aluminum, however, is exceptional in this respect, for almost all the metal–oxygen bonds that occur in soil minerals are strongly ionic. For example, Mg–O and Ca–O bonds are considered 75% to 80% ionic, whereas Na–O and K–O bonds are 80% to 85% ionic. Covalence thus plays a relatively minor role in determining the atomic structure of most soil minerals, aside from the important feature that

Si–O bonds, being 50% covalent, impart particular stability against mineral weathering, as discussed in Section 1.3.

Given this perspective on the chemical bonds in minerals, the two most useful atomic properties of the ions constituting soil minerals should be their valence and radius. Ionic valence is simply the ratio of the electric charge on an ionic species to the charge on the proton. Ionic radius, however, is a less direct concept, because the radius of a single ion in a solid cannot be measured. Ionic radius thus is a *defined quantity* based on the following three assumptions: (1) the radius of the bivalent oxygen ion (O^{2-}) in *all* minerals is 0.140 nm, (2) the sum of cation and anion radii equals the measured interatomic distance between the two ions, and (3) the ionic radius may depend on the coordination number, but otherwise is independent of the type of mineral structure containing the ion. The coordination number is the number of ions that are nearest neighbors of a given ion in a mineral structure. Table 2.1 lists standard cation radii calculated from crystallographic data under these three assumptions. Note that the radii depend on the valence (Z) as well as the coordination number (CN) of the metal cation. The radius decreases as the valence increases and electrons are drawn toward the nucleus, but it increases with increasing coordination number for a given valence. The coordination numbers found for cations in soil minerals are typically 4 or 6, and occasionally 8 or 12. The geometric arrangements of anions that coordination numbers represent are illustrated in Figure 2.1. Each of these arrangements corresponds to a regular geometric solid (a *polyhedron*, as shown in the middle row of Fig. 2.1). It is evident that the strength of the anionic electrostatic field acting on a cation will increase as its coordination number increases. This stronger anionic field draws the "electron cloud" of the cation more into the void space between the anions, thereby causing the cation radius to increase with its coordination number.

Two important physical parameters can be defined using the atomic properties listed in Table 2.1. The first parameter is *ionic potential* (or *IP*),

$$\mathrm{IP} = \frac{\mathrm{Z}}{\mathrm{IR}} \tag{2.1}$$

which is proportional to the coulomb potential energy at the periphery of a cation, as discussed in Section 1.2. The second parameter is *bond strength* (s), a more subtle concept from Linus Pauling,

$$\mathrm{s} = \frac{|\mathrm{Z}|}{\mathrm{CN}} \tag{2.2}$$

which is proportional to the electrostatic flux emanating from (or converging toward) an ion along one of the bonds it forms with its nearest neighbors. Given that the number of these latter bonds equals CN, it follows that *the sum of all bond strengths assigned to an ion in a mineral structure is equal to the absolute value of its valence* (i.e., |Z|). This characteristic property of bond strength is a special case of Gauss' law in electrostatics.

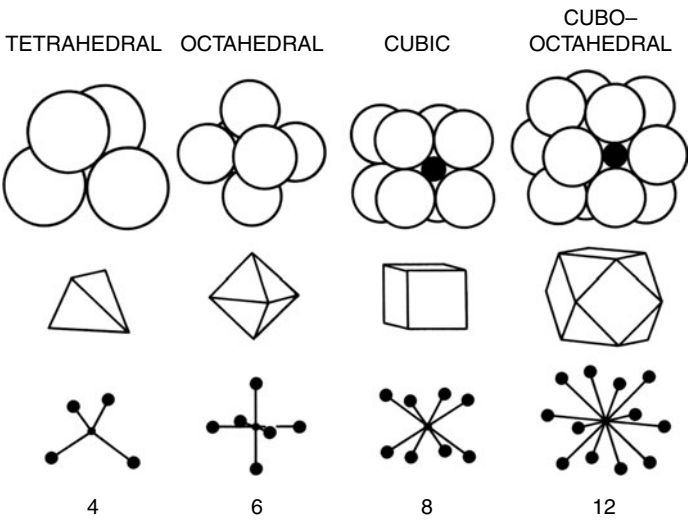

Figure 2.1. The principal coordination numbers for metal cations in soil minerals, illustrated by closely packed anion spheres (top), polyhedra enclosing a metal cation (middle), and "ball-and-stick" drawings (bottom).

The chemical significance of bond strength can be illustrated by an application to the four oxyanions discussed in Section 1.1: NO_3^-, SO_4^{2-}, CO_3^{2-}, and PO_4^{3-}. The strength of the bond between the central cation and one of the peripheral O^{2-} in each of the four oxyanions can be calculated using Eq. 2.2:

$$s = \frac{5}{3} = 1.67 \text{ vu } (NO_3^-) \qquad s = \frac{6}{4} = 1.50 \text{ vu } (SO_4^{2-})$$

$$s = \frac{4}{3} = 1.33 \text{ vu } (CO_3^{2-}) \qquad s = \frac{5}{4} = 1.25 \text{ vu } (PO_4^{3-})$$

where vu means valence unit, a conventional (dimensionless) unit for bond strength. Note that the sum of the bond strengths assigned to each central cation is equal to its valence (e.g., $3 \times 5/3 = 5$, the valence of N in the nitrate anion). But, because none of these bond strengths equals 2.0 (the absolute value of the valence of O^{2-}), any peripheral oxygen ion still has the ability to attract and bind an additional cationic charge external to the oxyanion. This conclusion follows specifically from Gauss' law, mentioned earlier, although it is also evident from the overall negative charge on each oxyanion. It is apparent that the strength of an additional bond formed between a peripheral oxygen ion and any external cationic charge will be smallest for nitrate (i.e., 2.00 – 1.67 = 0.33 vu) and largest for phosphate (i.e., 0.75 vu), with the resultant ordering: $NO_3^- < SO_4^{2-} < CO_3^{2-} < PO_4^{3-}$. This ordering is also the same as observed experimentally for the reactivity of these anions with positively

Table 2.1
Ionic radius (*IR*), coordination number (*CN*), and valence (*Z*) of metal and metalloid cations.[a]

Metal	*Z*	*CN*	*IR* (nm)	Metal	*Z*	*CN*	*IR* (nm)
Li	1	4	0.059	Co	2	6	0.075
	1	6	0.076		3	6	0.061
Na	1	6	0.102	Ni	2	6	0.069
Mg	2	6	0.072	Cu	2	4	0.057
Al	3	4	0.039		2	6	0.073
	3	6	0.054	Zn	2	6	0.074
Si	4	4	0.026	As	3	6	0.058
K	1	6	0.138		5	4	0.034
	1	8	0.151	Sr	2	6	0.118
	1	12	0.164	Zr	4	8	0.084
Ca	2	6	0.100	Mo	6	4	0.041
	2	8	0.112	Ag	1	6	0.115
Ti	4	6	0.061	Cd	2	6	0.095
Cr	3	6	0.062	Cs	1	6	0.167
	6	4	0.026		1	12	0.188
Mn	2	6	0.083	Ba	2	6	0.135
	3	6	0.065	Hg	1	6	0.119
	4	6	0.053		2	6	0.102
Fe	2	6	0.078	Pb	2	6	0.119
	3	6	0.065		4	6	0.078

[a] Shannon, R. D. (1976) Revised effective ionic radii and systematic studies of interatomic distances in halides and chalcogenides. *Acta. Cryst.* **A32**:751–767.

charged sites on particle surfaces (noted in Section 1.1), and it is the order of increasing affinity of the anions for protons in aqueous solution, as indicated by the pH value at which they will bind a single proton. The example given here shows that bond strength can be pictured as the absolute value of an *effective valence* of an ion, assigned to one of its bonds under the constraint that the sum of all such effective valences must equal the absolute value of the actual valence of the ion.

Bond strength usually has only one or two values for cations of the Class A metals discussed in Section 1.2, because these metals typically exhibit only one or two preferred coordination numbers in mineral structures, but bond strength can be quite variable for cations of Class B metals. This happens because of their large polarizability (i.e., large deformability of their electron clouds), which allows them access to a broader range of coordination numbers. A prototypical example is the Class B metal cation Pb^{2+}, for which coordination numbers with O^{2-} ranging from 3 to 12 are observed, with the corresponding bond strengths then varying from 0.67 to 0.17 vu, according to Eq. 2.2. This kind of broad variability and the tendency of cation

radii to increase with coordination number, as noted earlier, suggest that an inverse relationship should exist between the ionic radius of Pb^{2+} and its bond strength (an idea also from Linus Pauling). Systematic analyses of thousands of mineral structures have shown that the exponential formula

$$s = \exp [27.03 (R_0 - R)] \tag{2.3}$$

provides an accurate mathematical representation of how bond strength s decreases with increasing length of a bond (R, in nanometers) between a metal cation and an oxygen ion. Values of the parameter, R_0, the metal cation–oxygen ion bond length that, for a given cation valence, would yield a bond strength equal to 1.0 vu, are listed in Table 2.2 for the metal and metalloid cations in Table 2.1. If the bond strength of Pb^{2+} ranges from 0.67 to 0.17 vu, one finds with Eq. 2.3 and $R_0 = 0.2112$ nm, introduced from Table 2.1, that the corresponding range of the Pb–O bond length in minerals is from 0.226 to 0.277 nm.

Seen the other way around, as a means for calculating bond strength from a measured value of R, Eq. 2.3 provides an alternative to Eq. 2.2. As an example,

Table 2.2
Bond valence parameter R_0 (Eq. 2.3) for metals and metalloids coordinated to oxygen.[a]

Metal	*Z*	R_0 (nm)	Metal	*Z*	R_0 (nm)
Li	1	0.1466	Ni	2	0.1654
Na	1	0.1803	Cu	2	0.1679
Mg	2	0.1693	Zn	2	0.1704
Al	3	0.1651	As	3	0.1789
Si	4	0.1624		5	0.1767
K	1	0.2132	Sr	2	0.2118
Ca	2	0.1967	Zr	4	0.1928
Ti	4	0.1815	Mo	6	0.1907
Cr	3	0.1724	Ag	1	0.1842
	6	0.1794	Cd	2	0.1904
Mn	2	0.1790	Cs	1	0.2417
	3	0.1760	Ba	2	0.2285
	4	0.1753	Hg	2	0.1972
Fe	2	0.1734	Pb	2	0.2112
	3	0.1759	Pb	4	0.2042
Co	2	0.1692			
	3	0.1634			

[a]Brown, I. D., and D. Alternatt. (1985) Bond-valence parameters obtained from a systematic analysis of the inorganic crystal structure database. *Acta. Cryst.* **B41**:244.
The average standard deviation of R_0 in this table is 0.0042 nm.

consider Al^{3+}, for which Eq. 2.3 takes on the form

$$s = \exp [27.03(0.1651 - R)] \tag{2.4}$$

where R is now the length of an Al–O bond in nanometers. In the aluminum oxide mineral corundum (Al_2O_3), Al^{3+} is in octahedral coordination with O^{2-}. Two different Al–O bond lengths are actually observed in this mineral (0.185 nm and 0.197 nm), corresponding to *s* values of 0.584 and 0.422 vu respectively. These two bond strengths bracket the ideal value of 0.50 calculated with Eq. 2.2 using $Z = 3$, $CN = 6$. When bond strength is calculated with Eq. 2.3 instead of Eq. 2.2, it is termed *bond valence,* not only to avoid confusion with the original Pauling definition, but also to emphasize its chemical interpretation as an effective valence of the ion to which it is assigned.

The electrostatic picture of ionic solids also has significant implications for what kinds of atomic structures these solids can have. The structures of most of the minerals in soils can be rationalized on the physical grounds that the atomic configuration observed is that which tends to minimize the total electrostatic energy. This concept has been formulated in a most useful fashion through a set of descriptive statements known as the *Pauling Rules:*

Rule 1: A polyhedron of anions is formed about each cation. The cation–anion distance is determined by the sum of the respective radii, and the coordination number is determined by the radius ratio of cation to anion.

Minimum radius ratio	Coordination number
1.00	12
0.732	8
0.414	6
0.225	4

Rule 2: In a stable crystal structure, the sum of the strengths of the bonds that reach an anion from adjacent cations is equal to the absolute value of the anion valence.

Rule 3: The cations maintain as large a separation as possible from one another and have anions interspersed between them to screen their charges. In geometric terms, this means that polyhedra tend *not* to share edges or especially faces. If edges are shared, they are shortened relative to the unshared edges.

Rule 4: In a structure comprising different kinds of cation, those of high valence and small coordination number tend not to share polyhedron elements with one another.

Rule 5: The number of essentially different kinds of ion in a crystal structure tends to be as small as possible. Thus, the number of

different types of coordination polyhedra in a closely packed array of anions tends to be a minimum.

Pauling Rule 1 is a statement that has the same physical meaning as Figure 2.1. The anion polyhedra mentioned in the rule are shown in the middle of the figure, and the bottom row of "ball-and-stick" cartoons shows the cation–anion bonds with lengths that are determined by the ionic radii. The radius of the smallest sphere that can reside in the central void created by closely packing anions in the four ways shown at the top of the figure can be calculated with the methods of Euclidean geometry. It turns out that this radius is always proportional to the radius of the coordinating anion. For example, in the case of tetrahedral coordination, the smallest cation sphere that can fit inside the four coordinating anions has a radius that is 22.5% of the anion radius, and for six coordinating anions, it is 41.4% of the anion radius. These minimum cation radii are listed as decimal fractions in the table that accompanies Pauling Rule 1. Specific examples of the cation-to-oxygen radius ratio can be calculated with the *IR* data in Table 2.1 and the defined O^{2-} radius of 0.140 nm. Any cation with a coordination number of 6, for example, should have an ionic radius ≥ 0.058 nm ($= 0.414 \times 1.40$). This is the case for all but two of the *IR* values in the table for CN $= 6$, illustrating the important further point that that Pauling Rules are good *approximations* based on a strictly electrostatic viewpoint.

Pauling Rule 2 will be recognized as a restatement of Gauss' law in terms of bond strength defined in Eq. 2.2. For most soil minerals, the anion to which the rule is applied is O^{2-}, although OH^-, CO_3^{2-}, and SO_4^{2-} also figure importantly (Table 1.3). As an example, consider the oxygen ions in quartz (SiO_2), which are coordinated to Si^{4+} ions. The radius of Si^{4+} is 0.026 nm, and its usual coordination number is 4. It follows from Eq. 2.2 that $s = 1.0$ for Si^{4+}. Because the absolute value of the valence of O^{2-} is 2, Pauling Rule 2 then permits only two Si^{4+} to bond to an O^{2-} in SiO_2. This means that each O^{2-} in quartz must serve as the corner of no more than two silica tetrahedra. Hypothetical atomic structures for quartz that would involve, say, O^{2-} at the corners of three tetrahedra linked together are thus ruled out.

A more subtle example of Pauling Rule 2 occurs in the structure of the iron oxyhydroxide mineral goethite (FeOOH). The radius of Fe^{3+} is 0.065 nm and, by Pauling Rule 1, its coordination number with O^{2-} must be 6 ($0.065 \div 0.140 = 0.464 > 0.414 \Rightarrow$ octahedral coordination). Therefore, s $= 0.5$ for Fe^{3+}, and four Fe^{3+} should bond to each O^{2-} in the goethite structure, according to Pauling Rule 2. However, inspection of the goethite structure reveals that each O^{2-} is bonded to *three* Fe^{3+}, not four (Fig. 2.2). The proton in the goethite structure can be used to provide a cation for a fourth bond to O^{2-}, but because there are twice as many O as H in goethite, each proton must be *shared* between two O^{2-} to satisfy Pauling Rule 2. If this is the case, then each proton will be doubly coordinated with O^{2-}, and its corresponding bond strength will be s $= \frac{1}{2} = 0.5$,

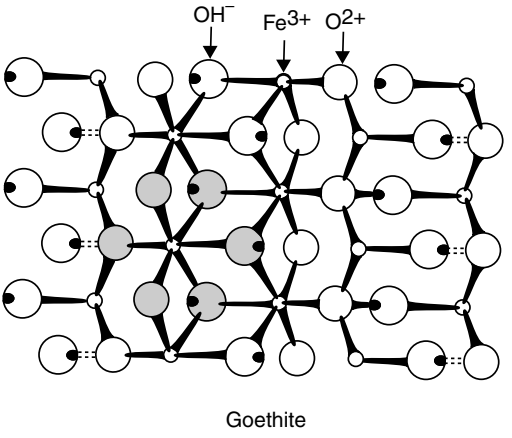

Figure 2.2. "Ball-and-stick" drawing showing the atomic structure of goethite. Note that the coordination number for O^{2-} and OH^{-} is equal to three.

as required. This sharing of a proton between two oxygens is termed *hydrogen bonding* (Fig. 2.2), by analogy with electron sharing in covalent bonding.

Hydrogen bonds seldom involve the proton placed symmetrically between two oxygens, but instead have one H–O bond significantly shorter (and stronger) than the other. The stronger H–O bond is about 0.095 nm in length and has a bond valence described mathematically by Eq. 2.3, with $R_0 = 0.0882$ nm, thus yielding $s = 0.83$ vu. By Gauss' law, the strength of the weaker bond must be 0.17 vu, because $Z = 1$ for the proton. Corresponding to these deviations from the ideal value, $s = 0.5$ vu, expected for a proton situated at the midpoint between two oxygens that share it, are those of the Fe^{3+} bond valences in goethite, which actually range from 0.377 to 0.600 vu because the Fe–O bond lengths vary from 0.212 to 0.195 nm [Eq. 2.3 with $R_0 = 0.1759$ nm (Table 2.2)]. Pauling Rule 2 can be satisfied either by three long Fe–O bonds combined with the stronger H–O bond or by three short Fe–O bonds combined with the weaker H–O bond.

Pauling Rule 3 reflects coulomb repulsion between cations. The repulsive electrostatic interaction between the cations in a crystal is weakened effectively, or *screened,* by the negatively charged anions in the coordination polyhedra of the cations. If the cations have a large valence, as does, for example, Si^{4+}, then the polyhedra can do no more than share corners if the cations are to be kept as far apart as possible in a structural arrangement that achieves the lowest possible total electrostatic energy. An example of a *sheet* of silica tetrahedra sharing corners is shown in Figure 2.3. If the cation valence is somewhat smaller, as it is for Al^{3+}, the sharing of polyhedron edges becomes possible. Figure 2.3 also shows this kind of sharing for a sheet of octahedra comprising six anions (e.g., O^{2-}) bound to a metal cation (e.g., Al^{3+}). Edge sharing brings

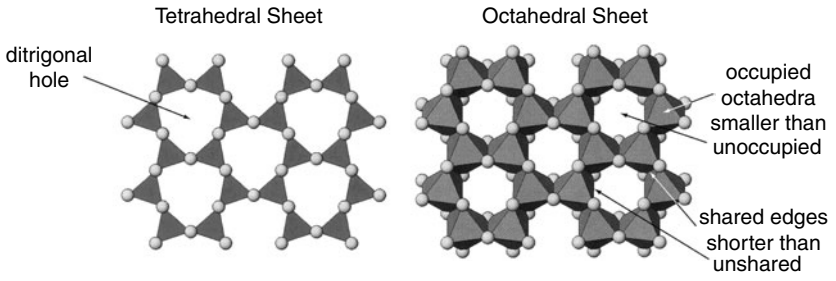

Figure 2.3. (A, B) Sheet structures in soil minerals formed by linking tetrahedra at corners (A) or octahedra along edges (B). Reprinted with permission from Schulze, D. G. (2002) An introduction to soil mineralogy, pp. 1–35. In: J. B. Dixon and D. G. Schulze (eds.), *Soil mineralogy with environmental applications.* Soil Science Society of America, Madison, WI.

the cations closer together than does corner sharing, however, so the task of charge screening by the anions is made more difficult. They respond to this by approaching one another slightly along the shared edge to enhance screening. Doing so, they necessarily shorten the edge relative to unshared edges of the polyhedra (Fig. 2.3), which is why there are short and long Al–O and Fe–O bonds in oxide minerals such as corundum (Al_2O_3) and goethite (FeOOH).

Pauling Rules 4 and 5 continue in the spirit of Rule 3. They reflect the fact that stable ionic crystals containing different kinds of cation cannot tolerate much sharing of the coordination polyhedra or much variability in the type of coordination environment. These and the other three Pauling Rules serve as useful guides to a molecular interpretation of the chemical formulas for soil minerals.

2.2 Primary Silicates

Primary silicates appear in soils as a result of deposition processes and from the physical disintegration of parent rock material. They are to be found mainly in the sand and silt fractions, except for soils at the early to intermediate stages of the Jackson–Sherman weathering sequence (Table 1.7), wherein they can survive in the clay fraction as well. The weathering of primary silicates contributes to the native fertility and electrolyte content of soils. Among the major decomposition products of these minerals are the soluble metal cation species Na^+, Mg^{2+}, K^+, Ca^{2+}, Mn^{2+}, and Fe^{2+} in the soil solution. The metal cations Co^{2+}, Cu^{2+}, and Zn^{2+} occur as trace elements in primary silicates (Table 1.4) and thus are also released to the soil solution by weathering. These *free-cation* species are readily bioavailable and, except for Na^+, are essential to the nutrition of green plants. The major element cations—Na^+, Mg^{2+}, and Ca^{2+}—provide a principal input to the electrolyte content in soil solutions.

The names and chemical formulas of primary silicate minerals important to soils are listed in Table 2.3. The fundamental building block in the atomic

Table 2.3
Names and chemical formulas of primary silicates found in soils.

Name	Chemical formula	Mineral group
Forsterite	Mg_2SiO_4	Olivine
Fayalite	Fe_2SiO_4	Olivine
Chrysolite	$Mg_{1.8}Fe_{0.2}SiO_4$	Olivine
Enstatite	$MgSiO_3$	Pyroxene
Orthoferrosilite	$FeSiO_3$	Pyroxene
Diopside	$CaMgSi_2O_6$	Pyroxene
Tremolite	$Ca_2Mg_5Si_8O_{22}(OH)_2$	Amphibole
Actinolite	$Ca_2Mg_4FeSi_8O_{22}(OH)_2$	Amphibole
Hornblende	$NaCa_2Mg_5Fe_2AlSi_7O_{22}(OH)$	Amphibole
Muscovite	$K_2[Si_6Al_2]Al_4O_{20}(OH)_4$	Mica
Biotite	$K_2[Si_6Al_2]Mg_4Fe_2O_{20}(OH)_4$	Mica
Phlogopite	$K_2[Si_6Al_2]Mg_6O_{20}(OH)_4$	Mica
Orthoclase	$KAlSi_3O_8$	Feldspar
Albite	$NaAlSi_3O_8$	Feldspar
Anorthite	$CaAl_2Si_2O_8$	Feldspar
Quartz	SiO_2	Silica

structures of these minerals is the silica tetrahedron: SiO_4^{4-}. Silica tetrahedra can occur as isolated units, in single or double chains linked together by shared corners (Pauling Rules 2 and 3), in sheets (Fig. 2.3), or in full three-dimensional frameworks. Each mode of occurrence defines a class of primary silicate, as summarized in Figure 2.4.

The *olivines* comprise individual silica tetrahedra in a structure held together with bivalent metal cations like Mg^{2+}, Fe^{2+}, Ca^{2+}, and Mn^{2+} in octahedral coordination. Solid solution (see Section 1.3) of the minerals forsterite and fayalite (Table 2.3) produces a series of mixtures with specific names, such as chrysolite, which contains 10 to 30 mol% fayalite. As discussed in Section 1.3, olivines have the smallest Si-to-O molar ratio among the primary silicates and, therefore, they feature the least amount of covalence in their chemical bonds. Their weathering in soil is relatively rapid (timescale of years), beginning along cracks and defects at the crystal surface to form altered rinds containing oxidized-iron solid phases and smectite (Table 1.3). More extensive leaching can result in congruent dissolution (see Problem 11 in Chapter 1) or can produce kaolinite instead of smectite, the formation of either of these clay minerals requiring a proximate source of Al, because none exists in olivine (except possibly as a trace element).

The *pyroxenes* and *amphiboles* contain either single or double chains of silica tetrahedra that form the repeating unit $Si_2O_6^{4-}$ or $Si_4O_{11}^{6-}$, respectively, with Si-to-O ratios near 0.33 to 0.36 (Fig. 2.4). The amphiboles feature isomorphic substitution of Al^{3+} for Si^{4+} (Table 2.3), and both mineral groups harbor a variety of bivalent metal cations, as well as Na^+, in octahedral

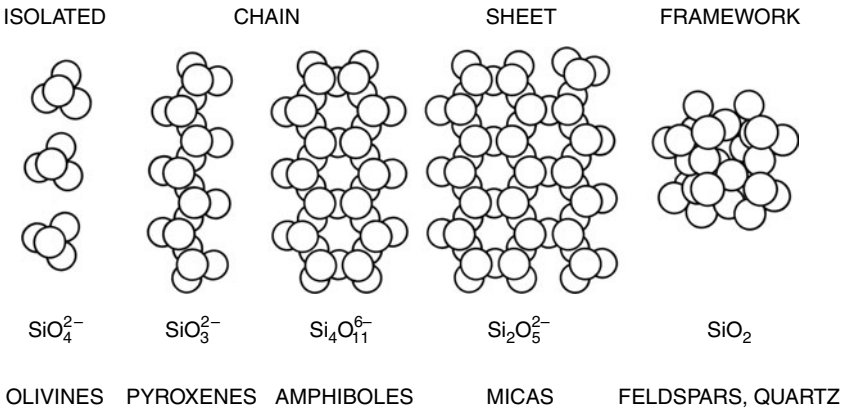

Figure 2.4. Primary silicates classified by the geometric arrangement of their silica tetrahedra.

coordination with O^{2-} to link the silica chains together. The weathering of these silicates is complex, with smectite and kaolinite, along with Al and Fe(III) oxides, being the principal secondary minerals emerging near structural defect sites where mineral dissolution begins. Hydrolysis and protonation, along with oxidation of Fe(II), are the main weathering mechanisms of olivines, pyroxenes, and amphiboles, although complexation (e.g., by oxalate) plays a dominant role when weathering is governed by microorganisms, such as bacteria or fungi.

The *micas* are built up from two sheets of silica tetrahedra ($Si_2O_5^{2-}$ repeating unit) fused to each planar side of a sheet of metal cation octahedra (Fig. 2.3). The octahedral sheet typically contains Al, Mg, and Fe ions coordinated to O^{2-} and OH^-. If the metal cation is trivalent, only two of the three possible cationic sites in the octahedral sheet can be filled to achieve charge balance and the sheet is termed *dioctahedral*. If the metal cation is bivalent, all three possible sites are filled and the sheet is *trioctahedral*. Isomorphic substitution of Al for Si, Fe(III) for Al, and Fe or Al for Mg occurs typically in the micas, along with the many trace element substitutions mentioned in Table 1.4.

Muscovite and biotite are the common soil micas, the former being dioctahedral and the latter trioctahedral (Table 2.3). In both minerals, Al^{3+} substitutes for Si^{4+}. The resulting charge deficit is balanced by K^+, which coordinates to 12 oxygen ions in the cavities of two opposing tetrahedral sheets belonging to a pair of mica layers stacked on top of one another. Thus the K^+ links adjacent mica layers together. It is these linking cations that are removed first as crystallite edges become frayed and, therefore, vulnerable to penetration by water molecules and competing soil solution cations during the initial stage of weathering (Fig. 2.5), which is accelerated by rhizosphere microorganisms that consume K^+ from the vicinal soil solution and release

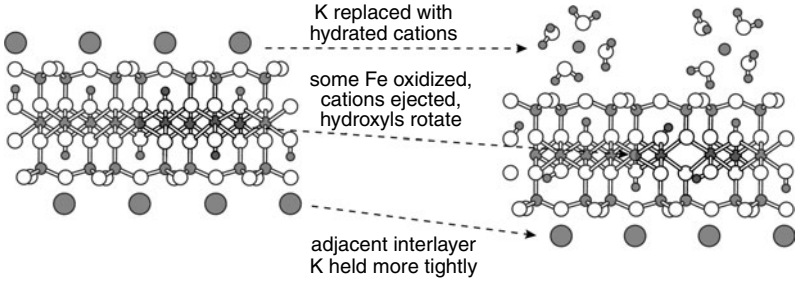

Figure 2.5. Some pathways of the initial stage of weathering of the trioctahedral mica, biotite. There is a loss of interlayer K^+ and oxidation of Fe^{2+} in the octahedral sheet, with consequent rotation of structural OH. Reprinted with permission from Thompson, M. L., and L. Ukrainczyk. (2002) Micas, pp. 431–466. In: J. B. Dixon and D. G. Schulze (eds.), *Soil mineralogy with environmental applications.* Soil Science Society of America, Madison, WI.

organic acids that complex and dislodge Al exposed at crystallite edges. Ferrous iron in biotite is gradually oxidized to ferric iron and ejected to hydrolyze and form an Fe(III) oxyhydroxide precipitate. This, in turn, allows some structural OH groups in the octahedral sheet to rotate toward the now-vacant former Fe(II) sites, the OH protons thereby being rendered less effective at repelling the surviving K^+ between the biotite layers (Fig. 2.5). Under moderate leaching conditions, muscovite transforms to dioctahedral smectite (see Problem 13 in Chapter 1), whereas biotite transforms to trioctahedral vermiculite and goethite (or ferrihydrite). A possible reaction for this latter transformation is

$$\underset{\text{(biotite)}}{K_2[Si_6Al_2]Mg_3\,Fe(II)_3O_{20}(OH)_4(s)} + 2.7\,Mg^{2+} + 3.9\,H_2O(\ell)$$
$$+ 0.75\,O_2(g) = \underset{\text{(vermiculite)}}{K_{1.7}[Si_6Al_2]\,Mg_{5.7}Fe(III)_{0.3}\,O_{20}(OH)_4(s)}$$
$$+ \underset{\text{(goethite)}}{2.7\,FeOOH(s)} + 0.3\,K^+ + 5.1\,H^+ \qquad (2.5)$$

Note that the layer charge (see Section 1.3), as evidenced by the stoichiometric coefficient of K^+, decreases from 2.0 in biotite to 1.7 in vermiculite because of the oxidation of ferrous iron. Although this layer charge is balanced by K^+ in Eq. 2.5, Mg^{2+} is also a common interlayer cation in trioctahedral vermiculite. Under intensive leaching conditions, biotite will transform to kaolinite and goethite, as illustrated in Eq. 1.3. In this case, silica and Mg^{2+} are lost to the soil solution along with K^+. A comparison of Eqs. 1.3 and 2.5 shows that kaolinite formation is favored by acidity (H^+ is a reactant) and inhibited by soluble Mg^{2+} (a product), whereas vermiculite formation is inhibited by acidity (H^+ is a product) and favored by soluble Mg^{2+} (a reactant).

The atomic structure of the *feldspars* is a continuous, three-dimensional framework of tetrahedra sharing corners, as in quartz, except that some of the

tetrahedra contain Al instead of Si, with electroneutrality thus requiring either monovalent or bivalent metal cations to occupy cavities in the framework. These primary minerals, the most abundant in soils, have repeating units of either $AlSi_3\ O_8^-$, with Na^+ or K^+ used for charge balance, or $Al_2\ Si_2\ O_8^{2-}$, with Ca^{2+} used for charge balance (Table 2.3). Solid solution among the three minerals thus formed is extensive, with that between albite and anorthite being known as *plagioclase*, whereas that between albite and orthoclase termed simply *alkali feldspar*. The weathering of these abundant minerals in soils occurs on timescales of millennia.

Figure 2.6 illustrates this last point with measurements of the amounts of hornblende, plagioclase, and K-feldspar remaining (relative to quartz) in the surface (A in Fig. 2.6) and subsurface (B and C in Fig. 2.6) horizons of a soil chronosequence comprising Entisols, Mollisols, Alfisols, and Ultisols, the members of which ranged in age from two centuries to 3000 millennia, as determined by radioactive isotope dating methods. The graph in Figure 2.6 indicates that all three primary silicates were depleted during the first few hundred millennia of weathering and that the overall rate of depletion was in the order of hornblende > plagioclase > K-feldspar, with the surface horizon

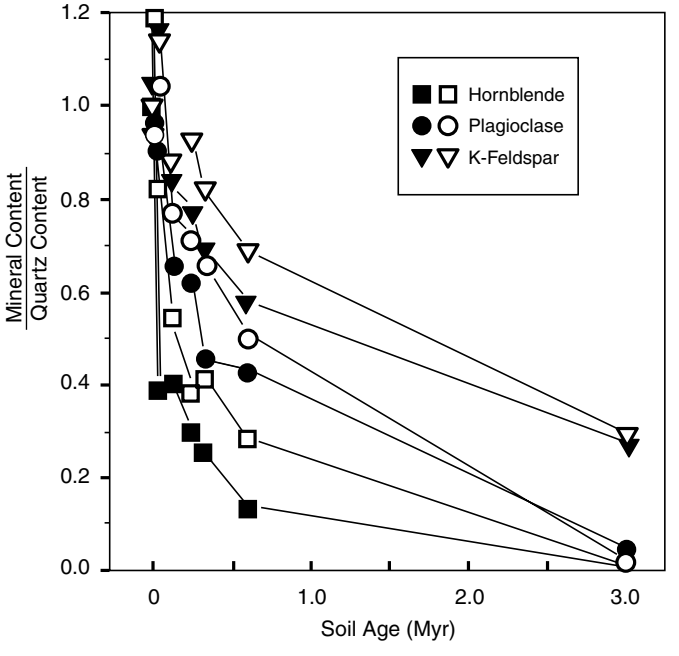

Figure 2.6. Depletion of amphiboles (hornblende) and feldspars (plagioclase and K-feldspar) with time during soil weathering. The ordinate is the content of primary silicate in the soil relative to that of quartz, which is assumed to be conserved. Data from White, A. F., et al. (1995) Chemical weathering rates of a soil chronosequence on granitic alluvium: I. *Geochim. Cosmochim. Acta* **60**:2533–2550.

showing more depletion than subsurface horizons. These trends are in keeping with the smaller Si-to-O ratio in amphiboles than in feldspars (see Section 1.3) and with the more intense weathering expected near the top of a soil profile.

Feldspar dissolution provides metal cations to the soil solution that figure importantly in the neutralization of acidic deposition on soils, the nutrition of plants, and the regulation of CO_2 concentrations. Bacteria and fungi enhance this dissolution process through the production of organic ligands (Eq. 1.4) and protons, particularly in the case of K-feldspar, which then serves as a source of K. Feldspars weather eventually to kaolinite (Eq. 1.2) or gibbsite (see Problem 12 in Chapter 1), but smectite also is a common secondary mineral product (see Problem 13 in Chapter 1):

$$\underset{\text{(orthoclase)}}{5\,KAlSi_3O_8(s)} + 4\,H^+ + 16\,H_2O(\ell) = \underset{\text{(beidellite)}}{K[Si_7Al]Al_4O_{20}(OH)_4(s)} + 8\,Si(OH)_4^0 + 4\,K^+ \qquad (2.6)$$

Note the consumption of protons and the production of silicic acid and soluble cations, as also observed in Eq. 1.2.

The general characteristics of primary silicate weathering illustrated by eqs. 1.2, 1.3, 1.4, 2.5, and 2.6 can be summarized as follows:

- Conversion of tetrahedrally coordinated Al to octahedrally coordinated Al
- Oxidation of Fe(II) to Fe(III)
- Consumption of protons and water
- Release of silica and metal cations

In the case of the micas, there is also an important reduction of layer charge accompanying the first two characteristics (Eq. 2.5 and Problem 13 in Chapter 1). From the weathering sequence in Table 1.7, one can conclude that soil development renders tetrahedral Al and ferrous iron unstable in response to continual throughputs of oxygenated fresh water (i.e., rainwater), which provides protons and, in return, receives soluble species of major elements. If these latter elements are not leached, the secondary silicates that characterize the intermediate stage of weathering will form, as in Eq. 2.6. If leaching is extensive, desilicated minerals characteristic of the advanced stage of weathering will begin to predominate in the clay fraction, as in eqs. 1.2 and 1.3.

2.3 Clay Minerals

Clay minerals are layer-type aluminosilicates that predominate in the clay fractions of soils at the intermediate to advanced stages of weathering. These

minerals, like the micas, are sandwiches of tetrahedral and octahedral sheet structures like those in Figure 2.3. This bonding together of the tetrahedral and octahedral sheets occurs through the apical oxygen ions in the tetrahedral sheet and produces a distortion of the anion arrangement in the final layer structure formed. The distortion occurs primarily because the apical oxygen ions in the tetrahedral sheet cannot be fit to the corners of the octahedra to form a layer while preserving the ideal hexagonal pattern of the tetrahedra. To fuse the two sheets, pairs of adjacent tetrahedra must rotate and thereby perturb the symmetry of the cavities in the basal plane of the tetrahedral sheet, altering them from hexagonal to ditrigonal (Fig. 2.3). Besides this distortion, the sharing of edges in the octahedral sheet shortens them (Pauling Rule 3, Fig. 2.3). These effects occur in the micas and in the clay minerals, both of whose atomic structures were first worked out by Linus Pauling (see Special Topic 2, at the end of this chapter). The clay minerals are classified into three *layer types*, distinguished by the number of tetrahedral and octahedral sheets combined to form a layer, and further into five *groups*, differentiated by the

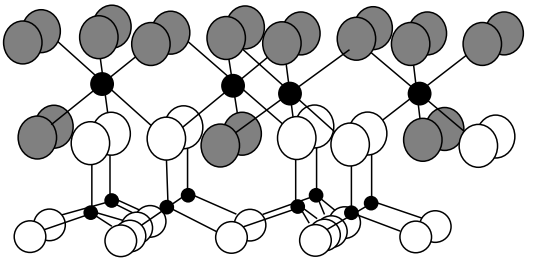

1:1 Layer Type

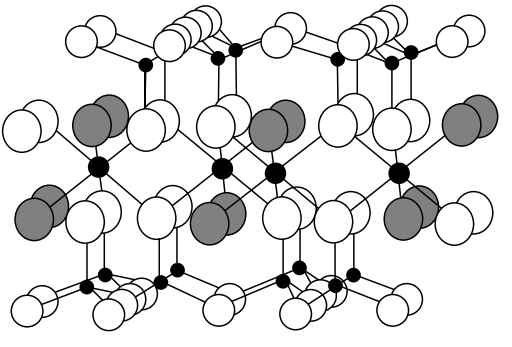

2:1 Layer Type

Figure 2.7. "Ball-and-stick" drawings of the atomic structures of 1:1 and 2:1 layer-type clay minerals.

Table 2.4
Clay mineral groups.[a]

Group	Layer type	Layer charge (x)	Typical chemical formula[b]
Kaolinite	1:1	< 0.01	$[Si_4]Al_4O_{10}(OH)_8 \cdot nH_2O$ ($n = 0$ or 4)
Illite	2:1	1.2–1.7	$M_x[Si_{6.8}Al_{1.2}]Al_3Fe_{0.25}Mg_{0.75}O_{20}(OH)_4$
Vermiculite	2:1	1.2–1.8	$M_x[Si_7Al]Al_3Fe_{0.5}Mg_{0.5}O_{20}(OH)_4$
Smectite[c]	2:1	0.4–1.2	$M_x[Si_8]Al_{3.2}Fe_{0.2}Mg_{0.6}O_{20}(OH)_4$
Chlorite	2:1 with hydroxide interlayer	Variable	$(Al(OH)_{2.55})_4\ [Si_{6.8}Al_{1.2}]Al_{3.4}Mg_{0.6}O_{20}(OH)_4$

[a]Guggenheim, S., et al. (2006) Summary of recommendations of nomenclature committees relevant to clay mineralogy. *Clays Clay Miner.* **54**:761–772.
[b][ ] indicates tetrahedral coordination; $n = 0$ is kaolinite and $n = 4$ is halloysite; H_2O = interlayer water; M = monovalent interlayer cation.
[c]Principally montmorillonite and beidellite in soils.

extent and location of isomorphic cation substitutions in the layer. The layer types are shown in Fig. 2.7, whereas the groups are described in Table 2.4.

The 1:1 layer type consists of one tetrahedral and one octahedral sheet. In soil clays, it is represented by the *kaolinite group*, with the generic chemical formula $[Si_4]Al_4O_{10}(OH)_8 \cdot nH_2O$, where the element enclosed in square brackets is in tetrahedral coordination and n is the number of moles of hydration water between layers. As is common for soil clay minerals, the octahedral sheet has two thirds of its cation sites occupied (dioctahedral sheet). Normally there is no isomorphic substitution for Si or Al in kaolinite group minerals, although low substitution of Fe for Al is sometimes observed in Oxisols, and poorly crystalline varieties of kaolinite are thought to have some substitution of Al for Si. Kaolinite group minerals are the most abundant clay minerals in soils worldwide, although, as implied in Table 1.7, they are particularly characteristic of highly weathered soils (Ultisols, Oxisols). Their typical particle size is less than 10 μm in diameter (fine silt and clay fractions), and their specific surface area ranges from 0.5 to 4.0×10^4 m^2 kg^{-1}, with the larger values being measured for poorly crystalline varieties. Aggregates of these clay minerals are observed as stacks of hexagonal plates if the layers are well crystallized, whereas elongated tubes with inside diameters on the order of 15 to 20 μm or more (or sometimes spheroidal particles) are found if the layers are poorly crystallized. (If the repeating structure based on the chemical formula of a solid phase persists throughout a molecular-scale region with a diameter that is at least as large as 3 nm, the solid phase is said to be *crystalline*. If structural regularity does not exist over molecular-scale distances this large, the solid phase is termed *poorly crystalline*.) The subgroup associated with the

tubular morphology contains interlayer water ($n = 4$ in the chemical formula) and is named *halloysite* (Table 2.4). Halloysite tends to be found under conditions of active weathering abetted by ample water, but it can dehydrate eventually to form more well-crystallized kaolinite ($n = 0$ in the chemical formula). The tubular morphology is thought to be an alternative structural response to tetrahedral–octahedral sheet misfit, wherein the tetrahedral sheet rolls around the octahedral sheet because interlayer water has prevented the tetrahedra from rotating as they do in kaolinite.

The oxygen ions in the basal plane of the tetrahedral sheet in kaolinite are bonded to a pair of Si^{4+}, whereas the apical oxygen ions are bonded to one Si^{4+} and two Al^{3+} in consonance with Pauling Rule 2 (Fig. 2.7). Similarly, the OH ions in the basal plane of the octahedral sheet are bonded to two Al^{3+}, as are the OH in the interior of the layer. Therefore, if the layer were infinite in lateral extent, it would be completely stable according to the Pauling rules. However, the oxygen and OH ions at the edge surfaces of a finite layer structure will always be missing some of their cation bonding partners, leading to the ability to bind additional cationic charge, as discussed for free oxyanions in Section 2.1. An exposed oxygen ion bound to a single Si^{4+} at an edge, for example, bears an excess charge of –1.0 vu and, therefore, requires a cation partner with a bond valence of 1.0 vu to be stable. This requirement can be met easily if a proton from aqueous solution becomes bound to the oxygen ion (Fig. 2.8). The situation is not as simple for an exposed OH ion, which bears an excess charge of –0.5 vu and thus requires a cation partner with a bond valence of 0.5 vu to be stable. Attraction of a proton from aqueous solution leads to the formation of $OH_2^{1/2+}$ at the edge surface, which is still not stable. The excess positive charge created can be neutralized in principle by a neighboring $OH_2^{1/2-}$, but this possibility clearly will be affected by soil solution pH. It turns out that the

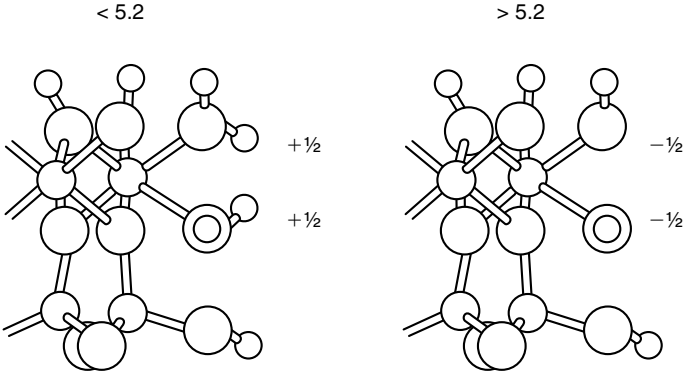

Figure 2.8. Atomic structure at the edge of a kaolinite layer exposed to water. As pH drops below 5.2, exposed Si–O^- and Al–$OH^{-1/2}$ each protonate to form Si–OH^0 and Al–$OH_2^{+1/2}$ respectively.

affinity of the kaolinite edge surface for protons leads to an electrically neutral condition at pH 5.2, with the surface being increasingly positively charged below this pH value and increasingly negatively charged above it. As was the case for the oxyanions considered in Section 2.1, failure to satisfy the Pauling Rules leads to reactivity with protons—in the present case, those in the soil solution contacting the edge surface of kaolinite.

The 2:1 layer type has two tetrahedral sheets that sandwich an octahedral sheet (Fig. 2.7). The three soil clay mineral groups with this structure are *illite, vermiculite,* and *smectite.* If a, b, and c are the stoichiometric coefficients of Si, octahedral Al, and Fe(III) respectively, in the chemical formulas of these groups, then

$$x \equiv \text{moles Al substituting for Si} + \text{moles Mg and Fe(II)} \text{ substituting for Al} \tag{2.7}$$

$$= (8 - a) + (4 - b - c) = 12 - a - b - c \tag{2.8}$$

is the *layer charge,* the number of moles of excess electron charge per chemical formula that is produced by isomorphic substitutions. As indicated in Table 2.4, the layer charge decreases in the order illite > vermiculite > smectite. The vermiculite group is further distinguished from the smectite group by a greater extent of isomorphic substitution in the tetrahedral sheet. Among the smectites, two subgroups also are distinguished in this way, those for which the substitution of Al for Si exceeds that of Fe(II) or Mg for Al (called *beidellite;* Eq. 2.6), and those for which the reverse is true (called *montmorillonite*). The smectite chemical formula in Table 2.4 represents montmorillonite. In any of these 2:1 minerals, the layer charge is balanced by cations that reside near or in the ditrigonal cavities of the basal plane of the oxygen ions in the tetrahedral sheet (Figs. 2.3 and 2.9). These interlayer cations are represented by M in the chemical formula of smectite (Table 2.4).

The layer charge in Eq. 2.7 is closely related to the *structural charge,* σ_0, defined by the equation

$$\sigma_0 = -(x/\mathrm{M_r}) \times 10^3 \tag{2.9}$$

where x is the layer charge and M_r is the relative molecular mass (see the Appendix). The units of σ_0 are moles of charge per kilogram ($\mathrm{mol_c\,kg^{-1}}$, see the Appendix). The value of $\mathrm{M_r}$ is computed with the chemical formula and known relative molecular masses of each element that appears in the formula. For example, in the case of the smectite with a chemical formula that is given in Table 2.4,

$$M_\mathrm{r} = \underset{\text{Si}}{8\,(28.09)} + \underset{\text{Al}}{3.2\,(27)} + \underset{\text{Fe}}{0.2\,(55.85)} + \underset{\text{Mg}}{0.6\,(24.3)} + \underset{\text{O}}{24\,(16)} + \underset{\text{H}}{4\,(1)} = \mathbf{725\ Da}$$

Therefore, according to Eq. 2.7 and the range of x in Table 2.4, σ_0 varies between –0.7 and –1.7 $mol_c\ kg^{-1}$ for smectites. In a similar way, σ_0 is found to vary from –1.9 to –2.8 $mol_c\ kg^{-1}$ for illites, and from –1.6 to –2.5 $mol_c\ kg^{-1}$ for vermiculites. These minerals are significant sources of negative structural charge in soils.

Particle sizes of the 2:1 clay minerals place them in the clay fraction, with illite and vermiculite typically occurring in larger aggregates of stacked layers than smectite, for which lateral particle dimensions around 100 to 200 nm are characteristic. Specific surface areas of illite average about $10^5\ m^2\ kg^{-1}$, whereas those of vermiculite and smectite can approach $8 \times 10^5\ m^2\ kg^{-1}$, depending on the number of stacked layers in an aggregate. The origin of this latter value, which is very large (equivalent to 80 $ha\ kg^{-1}$ clay mineral), can be seen by calculating the specific surface area (a_s) of an Avogadro number of unit cells (unit cells are the basic repeating entities in a crystalline solid) forming a layer of the smectite featured in Table 2.4:

$$\begin{aligned} a_s &= \text{surface area per unit cell } \times (N_A/M_r) \times 10^3 \\ &= 0.925\ nm^2 \text{ per cell } \times 10^{-18} m^2\ nm^{-2} \\ &\quad \times \frac{6.022 \times 10^{23}}{725\ g} \text{ cells } \times 10^3 g\ kg^{-1} \\ &= \mathbf{7.6 \times 10^5 m^2\ kg^{-1}} \end{aligned}$$

where $N_A = 6.022 \times 10^{23}$ is the Avogadro constant (also denoted L; see the Appendix) and the surface area of the smectite unit cell is calculated as twice the nominal surface area of one face in the crystallographic ab plane (i.e., twice 0.4627 nm^2), which is valid for a crystal layer with lateral dimensions (100–200 nm) that greatly exceed its thickness (only 1 nm for 2:1 clay minerals). This very large specific surface area pertains to particles that comprise a single crystal layer 100 to 200 nm in diameter. If, instead, n such layers are stacked to build an aggregate, the specific surface area is equal to the value found previously divided by n, because stacking a pair of layers together necessarily consumes the area of one basal surface of each. In aqueous suspensions, $n = 1$ to 3 for smectites with monovalent interlayer cations (e.g., Li^+, Na^+, K^+), whereas dehydrated smectites are found in aggregates with about 10 times as many stacked layers. Thus a_s for smectite aggregates can vary from nearly 80 $ha\ kg^{-1}$ to around 4 $ha\ kg^{-1}$.

The 2:1 layer type with a hydroxide interlayer is represented in soils by vermiculite or smectite with an Al–hydroxy polymer cation in the interlayer regions (Table 2.4), with the collective name for these subgroups being *pedogenic chlorite.* Formation of these clay minerals is mediated by acidic conditions, under which Al^{3+} is released by mineral dissolution, hydrolyzes, and replaces the interlayer cations in vermiculite or smectite, with incomplete hydrolysis resulting in a cationic Al–hydroxy polymer with a fractional

stoichiometric coefficient for OH < 3 instead of $Al(OH)_3$. Pedogenic chlorite is characteristic of highly weathered soils, such as Ultisols and Oxisols, but also is found in Alfisols and Spodosols. Whenever a complete, isolated gibbsite sheet [$Al(OH)_3$] forms in the interlayer region, the resulting mineral is termed simply *chlorite*.

Structural disorder in the 2:1 clay minerals listed in Table 2.4 is induced through isomorphic substitutions in their octahedral sheets (tables 1.5 and 2.4). More pronounced structural disorder exists in silica and in aluminosilicates that are freshly precipitated in soils undergoing active weathering, because these solid phases typically are excessively hydrated and poorly crystalline. Even among the more crystalline soil clay minerals, there is also wide variability in nanoscale order, with disorder created by dislocations (microcrevices between offset rows of atoms) and irregular stacking of crystalline unit layers. This kind of disorder exists, for example, in kaolinite and illite group minerals.

Poorly crystalline hydrated aluminosilicates, known collectively as *imogolite* and *allophane* (Table 1.3), are common in the clay fractions of soils formed on volcanic ash deposits (Andisols), but they can also be derived from many other kinds of parent material (e.g., granite or sandstone) under acidic conditions, regardless of temperature regime, if soluble Al and Si concentrations are sufficiently high and Al is not complexed with organic ligands, which interferes with precipitation (Eq. 1.4). Imogolite, having the chemical formula $Si_2Al_4O_{10} \cdot 5\,H_2O$, contains only octahedrally coordinated Al and exhibits a slender tubular particle morphology. The tubes are several micrometers long, with a diameter of about 2 nm, exposing a defective, gibbsitelike outer surface. The specific surface area of imogolite is comparable with—or even greater than—that of smectite. A surface charge develops from unsatisfied oxygen ion bond valences, similar to what occurs in kaolinite group minerals, but the pH value at which imogolite is electrically neutral is much higher (pH $\approx$ 8.4).

Allophane has the general chemical formula $Si_yAl_4O_{6+2y} \cdot n\,H_2O$, where $1.6 \leq y \leq 4$, $n \geq 5$ (Table 1.3). Thus it exhibits Al-to-Si molar ratios both larger and smaller than imogolite ($y = 2$) and it contains more bound water. Its specific surface area is also comparable with that of smectite and, like this latter clay mineral, a structural charge in allophane is possible because of isomorphic substitution of Al for Si in tetrahedral coordination, and charge development from unsatisfied oxygen ion bond valences occurs just as it does in kaolinite and imogolite. The pH value at which the protonation mechanism results in an electrically neutral surface varies inversely with the value of y in the chemical formula, decreasing from about pH 8.0 for $y = 2$ (termed the *proto-imogolite* allophane species) to about pH 5.4 for $y = 4$ (termed the *defect kaolinite* allophane species). Evidently, the increasing presence of Al results in stronger protonation, thus requiring higher pH for electrical neutrality, whereas that of Si has the opposite effect. The atomic structure of allophane is not well understood, but is thought in most cases to consist of fragments of imogolite combined with a 1:1 layer-type aluminosilicate that is riddled with vacant ion

sites and doped with Al in tetrahedral coordination. This defective structure promotes a curling of the layer into the form of hollow spheroids 3 to 5 nm in diameter with an outer surface that can contain many microapertures through which molecules or ions in the soil solution might invade. As this structural concept suggests, allophane often is found in association with kaolinite group minerals, especially halloysite.

Poorly crystalline kaolinite group minerals have been observed to precipitate in bacterial *biofilms*, which are layered organic matrices comprising extracellular polymers that enmesh bacterial cells along with nutrients and other chemical compounds. When minerals form in biofilms, the biofilms are termed *geosymbiotic microbial ecosystems* to emphasize the close spatial relationship that exists between the minerals and the microbes. Under highly anaerobic conditions at circumneutral pH in freshwater biofilms that contain a variety of different bacteria and filamentous algae, clay-size, hollow, spheroidal particles identified as poorly crystalline kaolinite group minerals appear to nucleate and grow on bacterial surfaces as a product of feldspar weathering (see Eq. 1.2). Similar observations have been reported for 2:1 layer-type clay minerals under active weathering conditions.

The 2:1 clay minerals, as well as pedogenic chlorite, imogolite, and allophone, all are expected to weather by hydrolysis and protonation to form kaolinite group minerals according to the Jackson–Sherman weathering sequence (Table 1.7):

$$\underset{\text{(beidellite)}}{\text{K[Si}_7\text{Al]Al}_4\text{O}_{20}\text{(OH)}_4(s)} + \text{H}^+ + \frac{13}{2}\text{H}_2\text{O}(\ell)$$

$$= \frac{5}{4}\underset{\text{(kaolinite)}}{\text{[Si}_4\text{]Al}_4\text{O}_{10}\text{(OH)}_8} + 2\ \text{Si(OH)}_4^0 + \text{K}^+ \qquad (2.10a)$$

$$\underset{\text{(pedogenic chlorite)}}{\text{(Al(OH)}_{2.5})_2\text{[Si}_7\text{Al]Al}_4\text{O}_{20}\text{(OH)}_4\text{(s)}} + 10\ \text{H}_2\text{O}(\ell) \qquad (2.10b)$$

$$= \underset{\text{(kaolinite)}}{\text{[Si}_4\text{]Al}_4\text{O}_{10}\text{(OH)}_8\text{(s)}} + 3\ \underset{\text{(gibbsite)}}{\text{Al(OH)}_3(s)} + 3\ \text{Si(OH)}_4^0$$

$$\underset{\text{(allophane)}}{\text{Si}_3\text{Al}_4\text{O}_{12}\cdot n\,\text{H}_2\text{O(s)}} + \frac{9}{2}\text{H}_2\text{O}(\ell)$$

$$= \frac{3}{4}\ \underset{\text{(kaolinite)}}{\text{[Si}_4\text{]Al}_4\text{O}_{10}\text{(OH)}_8\text{(s)}} + \underset{\text{(gibbsite)}}{\text{Al(OH)}_3\text{(s)}} + n\,\text{H}_2\text{O}(\ell) \qquad (2.10c)$$

Each of these reactions requires acidic conditions that are favored by freshwater and good drainage. The pedogenic chlorite reacting in Eq. 2.10b is an example of *hydroxy-interlayer beidellite* ($x = 1.0$), whereas *hydroxy-interlayer*

vermiculite ($x = 1.8$) is shown in Table 2.4. The allophane reactant in Eq. 2.10c is a *defect kaolinite* species.

2.4 Metal Oxides, Oxyhydroxides, and Hydroxides

Because of their great abundance in the lithosphere (Table 1.2), aluminum, iron, manganese, and titanium form the important oxide, oxyhydroxide, and hydroxide minerals in soils. They represent the *climax mineralogy* of soils, as indicated in Table 1.7. The most significant of these minerals, all of which are characterized by small particle size and low solubility in the normal range of soil pH values, can be found in Table 2.5, with representative atomic structures of some of them depicted in figures 2.9 and 2.10. For each type of metal cation, the Pauling Rules would indicate primarily octahedral coordination with oxygen or hydroxide anions.

Gibbsite [γ–$Al(OH)_3$], the only Al mineral listed in Table 2.5, is found commonly in Oxisols, Ultisols, Inceptisols, and Andisols, forming parallelepipeds 50 to 100 nm in length under conditions of warm climate and intense leaching that lead to Si removal from clay minerals and primary silicates, especially feldspars (see Table 1.7; Eqs. 2.10b, c; and Problem 12 in Chapter 1). Isomorphic substitutions do not appear to occur in this mineral. Inorganic anions, such as carbonate and silica, and organic ligands, including humic substances, disrupt the formation of gibbsite by complexing Al^{3+} (e.g., Eq. 1.7), and promote instead the precipitation of poorly crystalline Al oxyhydroxides with large specific surface areas (10–60 ha kg^{-1}). These highly reactive, disordered polymeric materials contribute significantly to the formation of stable aggregates in soils, often coating particle surfaces or entering between the layers of 2:1 layer-type clay minerals to form hydroxy-interlayer species (Table 2.4 and Eq. 2.9b).

Table 2.5
Metal oxides, oxyhydroxides, and hydroxides found commonly in soils.

Name	Chemical formula[a]	Name	Chemical formula[a]
Rutile	TiO_2	Hematite	α-Fe_2O_3
Birnessite	$M_xMn(IV)_aMn(III)_b\blacktriangle_cO_2^b$	Lepidocrocite	γ-FeOOH
Ferrihydrite	$Fe_{10}O_{15} \cdot 9\,H_2O$	Lithiophorite	$LiAl_2(OH)_6Mn(IV)_2Mn(III)O_6$
Gibbsite	γ-$Al(OH)_3$	Maghemite[c]	γ-Fe_2O_3
Goethite	α-FeOOH	Magnetite[c]	$FeFe_2O_4$

[a] γ denotes cubic close-packing of anions, whereas α denotes hexagonal close-packing.
[b] M = monovalent interlayer cation, $x = b + 4c$, $a + b + c = 1$, $\blacktriangle$ = cation vacancy.
[c] Some of the Fe(III) is in tetrahedral coordination.

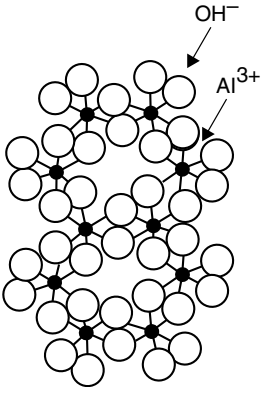

Figure 2.9. "Ball-and-stick" drawing of the atomic structure of gibbsite [γ-$Al(OH)_3$].

Gibbsite is a dioctahedral mineral comprising edge-sharing $Al(OH)_6$ in stacked sheets that are held together as an aggregate by hydrogen bonds that form between opposing OH groups oriented perpendicularly to the basal planes of the sheets. Hydrogen bonds also link the OH groups along the edges of the cavities lying within a single sheet (Fig. 2.9), adding to the distortion of the octahedra that is produced by the sharing of edges (Pauling Rule 3 and Fig. 2.3). According to Pauling Rule 2, the bond strength of Al^{3+} octahedrally coordinated to hydroxide ions is 0.5 and, therefore, each OH^- in gibbsite should be bonded to a pair of Al^{3+}, as indicated in Fig. 2.9 for the bulk structure. At the edges of a sheet, however, pairs of hydroxyls are exposed that

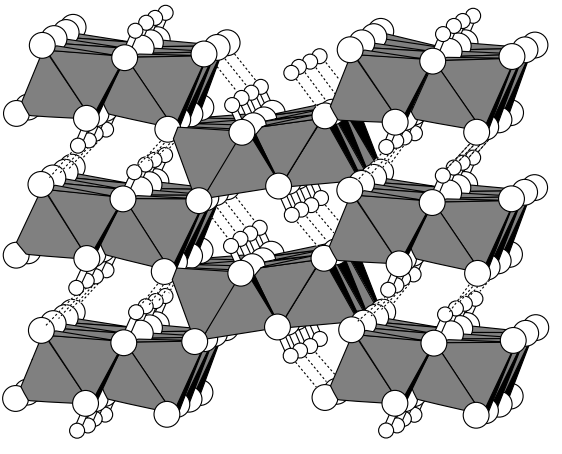

Figure 2.10. Polyhedral depiction of the atomic structure of goethite, with the double chains of Fe(III) octahedra lying perpendicular to the plane of the figure.

have unsatisfied bond valences. These hydroxyls lie along unshared octahedral edges and are located approximately 0.197 nm from the Al^{3+} to which they are coordinated, yielding an associated bond valence of 0.422 vu according to Eq. 2.4. This leaves an unsatisfied bond valence equal to −0.578 vu on each exposed hydroxyl. Adsorption of a proton by one OH, following the paradigm outlined for kaolinite edge surfaces (Fig. 2.8), then yields a more stable configuration of the hydroxyl pairs, which can be stabilized even further by hydrogen bonds with nearby water molecules in the soil solution. The pH value at which an electrically neutral gibbsite edge surface occurs turns out to be about 9.0, implying that this mineral bears a net positive charge over the entire normal range of soil pH values. By contrast, the edge surfaces of clay minerals typically bear a net negative charge above pH 5 to 7, depending on the type of clay mineral, again illustrating the stronger protonation of Al–OH groups relative to Si–OH groups that are exposed on edge surfaces.

Among the iron minerals listed in Table 2.5, *goethite* (α-FeOOH, named in honor of the German polymath, Johann Wolfgang von Goethe, who described iron oxides in the red soils of Sicily during the late 18th century) is the most abundant in soils worldwide, especially in those of temperate climatic zones. Its atomic structure (Fig. 2.10) comprises double chains of edge-sharing, distorted octahedra having equal numbers of O^{2-} and OH^{-} coordinated to Fe^{3+}, with each double chain then sharing octahedral corners with neighboring double chains. As discussed in Section 2.1, the Pauling Rules, supplemented by the more general concept of bond valence, are satisfied in this structure only because of hydrogen bonding between OH and O (Fig. 2.2). In soils, goethite crystallizes with relatively small particle size, exhibiting specific surface areas that range from 2 to 20 ha kg^{-1}.

Soils in warm, dry climatic zones tend to contain *hematite* (α-Fe_2O_3, named for its red-brown hue) in preference to goethite (which has a yellow-brown hue). Hematite has the same atomic structure as the Al oxide mineral corundum, mentioned in Section 2.1, with both having hexagonal rings of edge-sharing octahedra arranged in stacked sheets that are themselves linked through face-sharing octahedra. All this polyhedral sharing pushes the Fe^{3+} cations closer together and produces considerable structural distortion, as would be predicted from Pauling Rule 3. Hematite particles tend to have rather low specific surface areas (<10 ha kg^{-1}). Substantial isomorphic substitution of Al for Fe can occur in both goethite and hematite, the upper limit for the Al-to-(Al + Fe) molar ratio being 0.33 in goethite and half of this value in hematite. Aluminum substitution in these minerals is favored in soils under acidic conditions that produce abundant soluble Al without the interference of complexation by organic ligands or silica.

If organic ligands—especially humic substances—or soluble silica are at significant concentrations, then the crystallization of goethite or hematite is inhibited and poorly crystalline Fe(III) oxyhydroxides precipitate instead. This situation is especially characteristic of the rhizosphere, resulting in the formation of root-associated Fe(III) mineral mixtures known as *iron plaque*.

Ferrihydrite ($Fe_{10}O_{15} \cdot 9H_2O$, an approximate chemical formula, because up to half of the H may be in hydroxide ions, not water) is the most common of these materials, found typically in soils where biogeochemical weathering is intense, soluble Fe(II) oxidation is rapid, and water content is seasonally high (e.g., Andisols, Inceptisols, and Spodosols). This mineral, often detected along with goethite in soils, exhibits varying degrees of ordering of its Fe(III) octahedra, with many structural defects, and spheroidal particle diameters of a few nanometers, leading to specific surface areas of 20 to 40 ha kg^{-1}. Ferrihydrite can precipitate abiotically from oxic soil solutions at circumneutral pH, but its formation tends to be mediated by bacteria at acidic pH or under anaerobic conditions that slow Fe(II) oxidation significantly. Even at circumneutral pH under oxic conditions, bacterial cell walls can nucleate ferrihydrite (and goethite) precipitation after complexing dissolved Fe^{3+} cations and, in some cases, producing organic polymers that constrain precipitation to occur near the cell surface. Bacteria that thrive within biofilms either in highly acidic oxic environments, or in anaerobic environments at circumneutral pH, can oxidize Fe(II) enzymatically and rapidly enough to produce ferrihydrite at rates well above those for abiotic pathways. The resulting poorly crystalline mineral is encapsulated within extracellular organic polymers that keep it from fouling the bacterial surface while it also serves as fortification against predation of the organism. When polymeric matrices become fully encrusted with ferrihydrite within this geosymbiotic microbial ecosystem, they are eventually abandoned by the bacteria, which then begin to manufacture a new biofilm.

Magnetite [$Fe(II)Fe(III)_2O_4$], a mixed-valence iron oxide, contains Fe^{2+} and half of its Fe^{3+} in octahedral coordination with O^{2-}, with the remaining Fe^{3+} being in tetrahedral coordination. This mineral, named for its magnetic properties, is widespread in soils and can form both abiotically (e.g., inherited from soil parent material, or precipitated during the incongruent dissolution of ferrihydrite promoted by a reaction with dissolved Fe^{2+} cations) and biogenically (e.g., within *magnetotactic* bacteria that utilize this mineral for orientation and migration in the earth's magnetic field, or as a secondary precipitate under anaerobic conditions following the weathering of ferrihydrite by bacteria that oxidize organic matter). *Maghemite* (γ-Fe_2O_3), another magnetic mineral, is also widespread in soils of warm climatic zones, forming through the oxidation of magnetite or from the intense heating of goethite and ferrihydrite, as produced by fire. Like goethite, hematite, and ferrihydrite, Al substitution, with an upper limit as high as found for goethite, occurs in both magnetite and maghemite, the latter commonly arising from a heat-promoted transformation of Al-substituted goethite.

Another mixed-valence mineral that can be formed by either abiotic or bacterially mediated incongruent dissolution of ferrihydrite under anaerobic conditions is *green rust* [$(A^{-\ell} \cdot nH_2O)\ Fe(III)_xFe(II)_y(OH)_{3x+2y-\ell}$], which comprises a ferric–ferrous hydroxide sheet bearing a positive structural charge (because of ferric iron) that is balanced by hydrated anions ($A^{-\ell} \cdot nH_2O$), such as chloride ($x = 1, y = 3, \ell = 1$), sulfate, or carbonate ($x = 2, y = 4, \ell = 2$),

which reside in the interlayer region, analogous to the interlayer cations that balance the negative structural charge in 2:1 layer-type clay minerals (see Section 2.3 and Table 2.4). Also in parallel to the 2:1 clay minerals, individual sheets stack to form aggregates, with the stacking arrangement of the sheets being determined by the nature of the interlayer anion. Green rust occurs under alkaline conditions in poorly drained, biologically active soils that are subject to anaerobic conditions because of high water content (hydromorphic soils).

Birnessite [$M_xMn(IV)_aMn(III)_b\blacktriangle_cO_2$, where M is a monovalent interlayer cation, $a + b + c = 1$, and ▲ is an empty cation site in the octahedral sheet] is the most common manganese oxide mineral in soils, where it is often observed in fine-grained coatings on particle surfaces. Like gibbsite, it is a layer-type mineral with sheets that comprise mainly $Mn^{4+}O_6$ octahedra, but with significant isomorphic substitution by Mn^{3+} ($0 \leq b \leq 0.3$) and a generous population of cation vacancies ($0 \leq \blacktriangle \leq 0.2$), both of which induce a negative structural charge. In practice, isomorphic substitutions tend to offset cation vacancies, such that a range of birnessites exists, varying from those with only Mn^{3+} substitution (*triclinic birnessite*) to those with only cation vacancies (δ-MnO_2 or *vernadite*). The resulting layer charge, $x = b + 4c$, is compensated by protons and hydrated metal cations, including both Mn^{2+} and Mn^{3+}, that reside in the interlayer region, particularly near cation vacancies, each of which bears four electronic charges in the absence of protonation

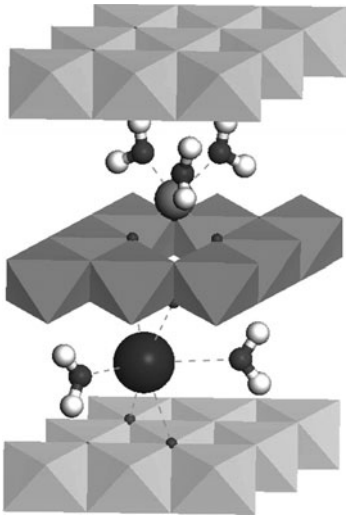

Figure 2.11. Polyhedral depiction of the local atomic structure in birnessite, showing a cation vacancy with charge-balancing, solvated interlayer cations (Mn^{3+} on top and K^+ on the bottom). Visualization courtesy of Dr. Kideok Kwon.

(Fig. 2.11). The layer charge is quite variable, but values near 0.25 are commonly observed, implying $\sigma_o \approx -3\ mol_c\ kg^{-1}$ (Eq. 2.8), which is comparable with the negative structural charge observed for 2:1 clay minerals. Birnessite typically forms poorly crystalline particles comprising a small number of stacked, defective sheets less than 10 nm in diameter. Specific surface areas of these particles range from 3 to 25 $ha\ kg^{-1}$, a range that is similar to soil goethites.

Birnessites precipitate in soils as a result of the oxidation of dissolved Mn^{2+}, which, if it occurs abiotically, is orders of magnitude slower than that of dissolved Fe^{2+} at circumneutral pH in the presence of oxygen. Bacteria and fungi that catalyze the oxidation of Mn(II) under these conditions enzymatically and rapidly (timescales of hours for bacterial oxidation vs. hundreds of days for abiotic oxidation) are widespread in nature, leading to the conclusion that soil birnessites are primarily of biogenic origin. Similar to bacteriogenic ferrihydrite, birnessites produced by bacteria often are found enmeshed within biofilms, where these highly reactive, poorly crystalline nanoparticles may serve to impede predation and sequester both toxic and nutrient metal cations. Geosymbiotic microbial ecosystems thus play an important role in the biogeochemical cycling of Al, Fe, and Mn in soils and natural waters.

2.5 Carbonates and Sulfates

The important carbonate minerals in soils include calcite ($CaCO_3$), dolomite [$CaMg(CO_3)_2$], nahcolite ($NaHCO_3$), trona [$Na_3H(CO_3)_2 \cdot 2\ H_2O$], and soda ($Na_2CO_3 \cdot 10\ H_2O$). Calcite may be, and dolomite appears often to be, a primary mineral in soils. Secondary calcite that precipitates from soil solutions enriched in soluble Mg coprecipitates with $MgCO_3$ to form *magnesian calcite,* $Ca_{1-y}Mg_yCO_3$, with the stoichiometric coefficient y typically well below 0.10. This mode of formation accounts for much of the secondary Mg carbonate found in arid-zone soils. Like secondary metal oxides and hydroxides, secondary Ca/Mg carbonates can occur as coatings on other minerals, in nodules or hardened layers, and as clay or silt particles. They are important repositories of inorganic C in Aridisols and Mollisols.

Pedogenic calcites are normal weathering products of Ca-bearing primary silicates (pyroxenes, amphiboles, feldspars) as well as primary carbonates. Their formation is favored in the rhizosphere, where bacteria and fungi mediate calcite precipitation, both through nucleation around excreted Ca^{2+} that has been complexed by cell walls and through increases in soil solution pH (>7.2) induced by enzymatically catalyzed reduction of nitrate, Mn, Fe, and sulfate or methane production, the last process being associated with pedogenic dolomite formation. As an example of primary mineral weathering to produce secondary calcite, the feldspar anorthite (Table 2.3) may be considered as follows:

$$\underset{\text{(anorthite)}}{CaAl_2Si_2O_8(s)} + 0.5\ Mg^{2+} + 3.5\ Si(OH)_4^0 + CO_2(g)$$
$$= \underset{\text{(smectite)}}{Ca_{0.5}[Si_{7.5}Al_{0.5}]Al_{3.5}Mg_{0.5}O_{20}(OH)_4(s)} + \underset{\text{(calcite)}}{CaCO_3(s)}$$
$$+ 0.5\ Ca^{2+} + 5\ H_2O(\ell) \qquad (2.11)$$

This incongruent dissolution reaction takes advantage of soluble Mg and silica available from weathering and of ubiquitous biogenic CO_2 in soils. Note that the reaction products are favored by abundant CO_2, because it is a reactant, and are inhibited by abundant H_2O, because it is one of the products. Thus, calcite formation can be prompted by elevated CO_2 concentration.

The formation of calcite from the dissolution of primary carbonates also is favored by abundant CO_2, but not as a source of dissolved carbonate ions. Instead, carbonic acid that is formed when CO_2 dissolves in the soil solution serves as a source of protons to aid in the dissolution of primary calcite or dolomite:

$$CO_2(g) + H_2O(\ell) = H_2CO_3^* = H^+ + HCO_3^- \qquad (2.12a)$$
$$CaCO_3(s) + H^+ = Ca^{2+} + HCO_3^- \qquad (2.12b)$$

where $H_2CO_3^*$ conventionally designates the sum of undissociated carbonic acid ($H_2CO_3^0$) and solvated CO_2 ($CO_2 \cdot H_2O$), because these two dissolved species are very difficult to distinguish by chemical analysis (see Problem 15 in Chapter 1). If soil leaching is moderate and followed by drying, the reaction in Eq. 2.11b is reversed and secondary calcite forms. Note that this reversal is favored by high pH (i.e., low proton concentration).

Calcium coprecipitation bivalent with Mn, Fe, Co, Cd, or Pb by sorption onto calcite is not uncommon (see Table 1.5). The trace metals Zn, Cu, and Pb also may coprecipitate with calcite by inclusion as the hydroxycarbonate minerals hydrozincite [$Zn_3(OH)_6(CO_3)_2$], malachite [$Cu_2(OH)_2CO_3$], azurite [$Cu_3(OH)_2(CO_3)_2$], or hydrocerrusite [$Pb_3(OH)_2(CO_3)_2$]. Under anoxic conditions that favor Mn(II), Fe(II), and abundant CO_2, rhodocrosite ($MnCO_3$) and siderite ($FeCO_3$) solid-solution formation is possible—in the absence of inhibiting sorption of humus by the nucleating solid phase, which also retards calcite precipitation. Green rust, the Fe(II)–Fe(III) hydroxy carbonate discussed in Section 2.4, can precipitate under these conditions as well, with CO_3^{2-} then being the interlayer anion.

Like secondary carbonates, Ca, Mg, and Na sulfates tend to accumulate as weathering products in soils that develop under arid to subhumid conditions, where evaporation exceeds rainfall (Table 1.7). The principal minerals in this group are gypsum ($CaSO_4 \cdot 2\,H_2O$), anhydrite ($CaSO_4$), epsomite ($MgSO_4 \cdot 7\,H_2O$), mirabilite ($Na_2SO_4 \cdot 10\,H_2O$), and thenardite (Na_2SO_4). Gypsum, similar to calcite, can dissolve and reprecipitate in a soil profile that

is leached by rainwater or irrigation water and can occur as a coating on soil minerals, including calcite. The Na sulfates, like the Na carbonates, form at the top of the soil profile as it dries through evaporation.

In highly acidic soils, sulfate, either produced through sulfide oxidation or introduced by amendments (e.g., gypsum), can react with the abundant Fe and Al in the soil solution to precipitate the minerals schwertmannite [$Fe_8O_8(OH)_6SO_4$], jarosite [$KFe_3(OH)_6(SO_4)_2$], alunite [$KAl_3(OH)_6(SO_4)_2$], basaluminite [$Al_4(OH)_{10}SO_4 \cdot 5\ H_2O$], or jurbanite ($AlOHSO_4 \cdot 5\ H_2O$). These minerals, in turn, may dissolve incongruently to form ferrihydrite and goethite or gibbsite upon further contact with a percolating, less acidic soil solution. Under similar acidic conditions, phosphate minerals such as wavellite [$Al_3(OH)_3(PO_4)_2 \cdot 5\ H_2O$], angellite [$Al_2(OH)_3PO_4$], barandite [$(Al,Fe)PO_4 \cdot 2\ H_2O$], and vivianite [$Fe_3(PO_4)_2 \cdot 8\ H_2O$] have been observed in soils, with the latter requiring anoxic conditions to precipitate, whereas the others require phosphoritic parent materials. As soil pH increases, Ca phosphates such as apatite [$Ca_3(OH,F)(PO_4)_3$] and octacalcium phosphate [$Ca_8H_2(PO_4)_6 \cdot 5\ H_2O$] tend to form, particularly if soluble phosphate has been introduced in abundance by soil amendments or wastewater percolation.

For Further Reading

Banfield, J. F., and K. H. Nealson (eds.). (1997) *Geomicrobiology: Interactions between microbes and minerals.* The Mineralogical Society of America, Washington, DC. The 13 chapters of this edited workshop volume provide a fine introduction to the important roles played by microorganisms in the formation and weathering of minerals in soils and aquatic environments.

Dixon, J. B., and D. G. Schulze (eds.). (2002) *Soil mineralogy with environmental applications.* Soil Science Society of America, Madison, WI. Chapters 6 through 22 of this standard reference work on soil minerals may be read to gain in-depth information about their structures, occurrence, and weathering reactions.

Essington, M. E. (2004) *Soil and water chemistry.* CRC Press, Boca Raton, FL. Chapter 2 of this comprehensive textbook may be consulted to learn more about the atomistic details of soil mineral structures through its many visualizations.

The following three specialized books offer a deeper understanding of the structure and reactivity of minerals in natural soils and aquatic systems, including those affected by pollution:

Cornell, R. M., and U. Schwertmann. (2003) *The iron oxides.* Wiley-VCH Verlag, Weinheim, Germany. This beautifully produced, exhaustive treatise on the iron oxides is an indispensable reference for anyone who wants to know specialized information.